JOURNAL OF COMPUTATIONAL PHYSICS 52, 427–447 (1983)

The Use of Distorting Grids and Flux Splitting to Model Axisymmetric Adiabatic Explosions

A. R. GARLICK

School of Mathematics, The University, Leeds LS2 9JT, United Kingdom

Received July 13, 1982; revised January 27, 1983

A method for solving the adiabatic gasdynamic equations on an arbitrarily distorting axisymmetric grid is described. It is used to apply the exact Rankine–Hugoniot relations at the outer boundary of the grid so that non-spherical explosions can be followed accurately and cheaply. It is found that a flux splitting algorithm gives a reliable difference scheme for the transformed equations. The method is illustrated by applying it to explosions in exponential atmospheres. The ideas behind a convenient approximation for such phenomena are used to check the accuracy both of the code and the approximation itself. Some further uses for this type of scheme are indicated.

1. INTRODUCTION

The primary motivation for the work described in this paper came from a single astrophysical problem: radiative supernova remnants in a non-uniform interstellar medium. A certain amount of energy (about 10^{51} ergs) is injected into a cold medium (density of order 10^{-24} g cm^{-3}) and forms a blast wave which is initially adiabatic. At later stages, however, radiative energy losses occur behind the blast wave shock in such a way that the density increases catastrophically. If the surrounding medium is uniform a one-dimensional spherically symmetric calculation can be made and Falle [1] has outlined the complex sequence of events. Falle uses a Lagrangian, characteristic scheme with shock fitting and variable mesh sizes, and this gives a good idea of the level of sophistication needed to model the very thin cooled region adequately.

For a non-uniform medium, the next stage is to make an axisymmetric calculation. During the adiabatic phase one can get away with conventional Eulerian difference schemes and calculations have been made by Garlick [2] for a magnetic explosion and by Falle and Garlick [3] for an explosion near a density discontinuity. In both cases the time-split FCT-SHASTA algorithm of Book, Boris and Hain [4] was used. Such schemes do not resolve very well the swept-up interstellar medium behind the shock, as was also noted by Chevalier and Gardner [5] for a supernova in an exponential atmosphere. It is clear, then, that these schemes will fail completely when cooling is important. A significant fraction of the mass is concentrated in a very thin

0021-9991/83 $3.00

layer which cannot be resolved on a two-dimensional Eulerian grid and, in particular, the fraction of the initial energy which is radiated cannot be calculated at all.

Precisely because of the thinness of this layer, however, it should be possible to find asymptotic analytic approximations for its dynamical behaviour. In principle we can use the results of such an analysis as boundary conditions on an interior flow which is approximately adiabatic. There are a number of ways in which this could be done and we shall not discuss them further. Whatever way is chosen, the first step is to construct a code in which the boundary of the numerical grid coincides at all times with position of the blast wave. Such a code is the subject of this paper and we use it here to model *adiabatic* explosions into a medium of varying density. The numerical asymptotic matching techniques will be the subject of future papers.

Of course, there are many other problems, both astrophysical and terrestrial, which this approach, and the present scheme, can be used for. Regions bounded by ionisation fronts or detonation waves form examples. It can be used to solve any two-dimensional hyperbolic system in a region with a free boundary and known or calculable external conditions and is accurate and cheap. Further, it gives the position of the free boundary explicitly.

The code requires the following ingredients in order to perform the function described above.

(a) *A Mapping.* A suitable time-dependent mapping is required which transforms the explosion (which possibly is of a peculiar shape) onto a simple numerical grid.

(b) *Equations.* The hydrodynamic equations must be written in the transformed coordinates in as useful a form as possible.

(c) *A Difference Scheme.* A robust and general difference scheme is needed which can cope with equations which may be rather far removed from the conventional hydrodynamic equations.

(d) *Boundary Conditions.* In addition to providing conditions on the interior physical variables, in this case the post-shock flow, the boundary conditions must determine how the grid evolves at each time step.

These ingredients are the subject of Sections 2–5 respectively.

In order to test the code we have looked at explosions in an exponential atmosphere. In the absence of reliable numerical solutions for this problem, we have used a somewhat roundabout checking procedure which also includes an assessment of the Laumbach–Probstein (LP) method. This method is simply to divide the explosion energy equally between each solid angle and to make a one-dimensional spherical calculation for each angle. In their paper [6] Laumbach and Probstein introduced a further approximation which we shall not need for the present work. At any rate the LP method is the principal analytic simplification for two-dimensional explosions. This approximation gives a slightly modified set of equations which we have also programmed. Since the two sets of equations are so similar we guess that the numerical method is of comparable accuracy in each case. The LP results for a

problem with known analytic solution then gives an indication of the accuracy of the method as a whole. They can also be compared with the results of the proper two-dimensional calculations as a test of the effectiveness of the LP method. All of this, together with the results of spherical runs, will be described in Section 6.

We summarise our conclusions in Section 7.

2. The Mapping

We work in cylindrical polar coordinates, (z, ϖ), where z is the axial distance and ϖ the cylindrical radius. In general the boundary of the region will be given in parametric form by the functions $z_b(\theta)$, $\varpi_b(\theta)$ and we want to map the interior of our region onto a suitable computational grid with coordinates (x, y). As far as possible we would like the mapping to satisfy the following (contradictory) set of constraints.

(i) It should be reasonably conformal since physical intuition suggests that in a hyperbolic system information will not be transferred properly between cells which are badly distorted.

(ii) The magnification should be such that the time step does not become too small under the Courant–Friedrichs–Lewy (CFL) condition. That is, locally fine grids should be avoided.

(iii) It must cope with peculiar shapes (which may be multivalued if z is expressed as a function of ϖ or vice versa).

(iv) It should be computationally cheap.

There is also a subsidiary problem as to the shape of the computational grid. Obviously a rectangular grid is inappropriate for the distorted spherical shapes expected and this suggests that the mapping should be done in two stages: first from the physical region to a disc, and then from the disc to the computational grid. Only the first stage would be time dependent and the parameter θ can then be the usual polar angle in the disc.

Now it is possible to solve problems (i), (iii) and (iv) simultaneously using a conformal mapping from the explosion to the unit disc. The Riemann Mapping Theorem assures us that it can be done non-singularly for all shapes and we can use Fast Fourier Transform (FFT) techniques to evaluate the mapping. However, there are problems in truncating the Fourier series when we discretise and, more fundamentally, it is known that property (ii) is very badly violated when the shape becomes appreciably non-spherical. This is described, for example, by Meiron, Orszag and Israeli [7] for the water wave problem which is not constrained by the CFL condition.

This leads us to consider the much simpler mapping:

$$z = z_0(t) + R(\theta, t) r \cos\theta,$$

$$\varpi = R(\theta, t) r \sin\theta.$$

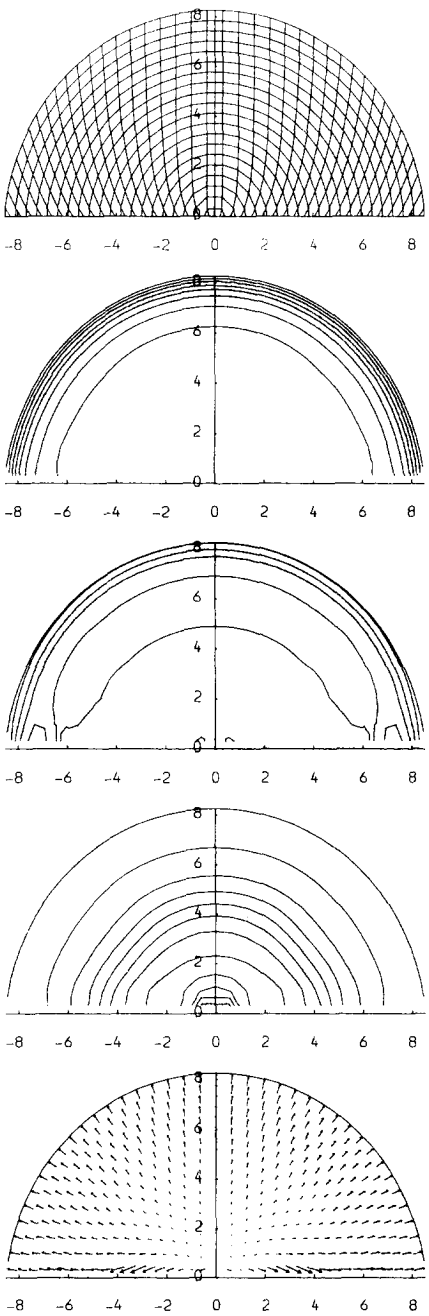

FIG. 1. Explosion into a uniform medium. From top to bottom are shown the computational grid, contour maps of density, pressure and temperature and a velocity plot. Each of the contour plots shows the first 20 contours in units of 0.5 for the density, 0.0005 for the pressure and 0.002 for the temperature (defined as p/ρ). See text for futher details.

We simply choose a point on the axis given by $z_0(t)$ and take radially distorted polar coordinates. Evidently we cannot cope with very peculiar shapes, but for these the conformal mapping would in any case be impractical. This maps the explosion into the unit half disc $0 \leqslant r \leqslant 1$, $0 \leqslant \theta \leqslant \pi$.

Computationally, too, this is cheap as we use bicubic splines to interpolate from the discrete form of $R(\theta)$ given by the boundary conditions to the various values of θ at which it is required internally, rather than the FFT required for conformal mapping. Even so, much time is spent on these calculations and no doubt computational expense could be significantly reduced with cruder interpolation.

The function $z_0(t)$ could be chosen so as to maximise the allowed time step though in all the calculations presented in this paper we take $z_0 = 0$, so that the origin remains at the initial site of the explosion.

Coming now to the mapping from the half disc to the grid, we wish to avoid the small time step which would result from a rectangular computational area associated with polar coordinates. We therefore use the following equal area mapping from the disc to a triangle:

$$r = x, \qquad 0 \leqslant x \leqslant 1,$$

$$\theta = \frac{\pi}{2}\left(1 + \frac{y}{x}\right), \qquad -x \leqslant y \leqslant x.$$

This transformation will thus not affect the time step and the distortion is everywhere moderate.

The effect of these mappings can be understood further by reference to the top parts of Figs. 1–3. These show the appearance of the distorted computational grid in physical space. In Fig. 1 the mapping from the half disc to the computational triangle is shown and in Figs. 2 and 3 the effect of the non-spherical distortion characteristic of an explosion in a density gradient is added. What is not obvious from these diagrams is that the expansion of the grid, due to the change of shape, is purely radial (unlike the expansion of the gas, of course), though it can be confirmed by tracing the image of radial lines.

The triangular computational area causes no particular problems as long as the x and y differences are made equal. With $\delta x = \delta y = 1/N$ the triangle contains N^2 cells. In all our runs we have $N = 20$. It can be seen that grid points are used very economically compared with conventional schemes, and since the flow behind the blast wave will normally be quite smooth it can easily be resolved with such a low value of N.

3. The Equations

We now consider the gasdynamic equations transformed to our computational grid. In the next section we use a difference scheme which exploits the conservative properties of the equations and so we would like them to be in conservation form as

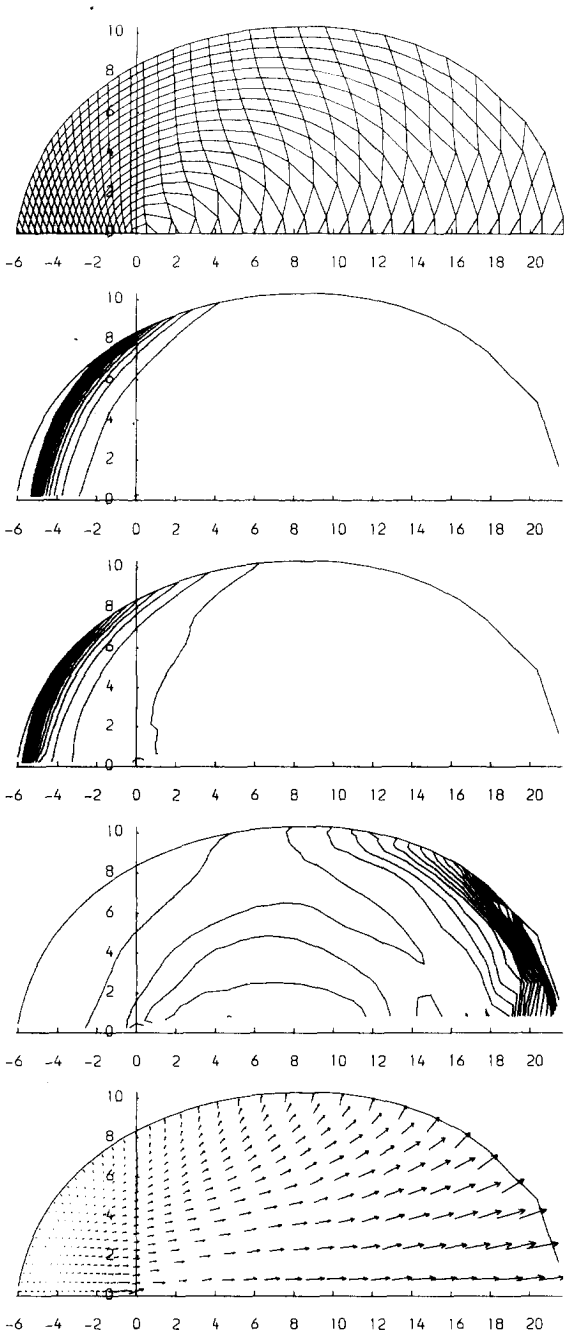

FIG. 2. As Fig. 1 for an explosion into an exponential atmosphere, $\rho_0 = \exp(-z/2)$. Units as Fig. 1, except velocity vectors are drawn at half the scale.

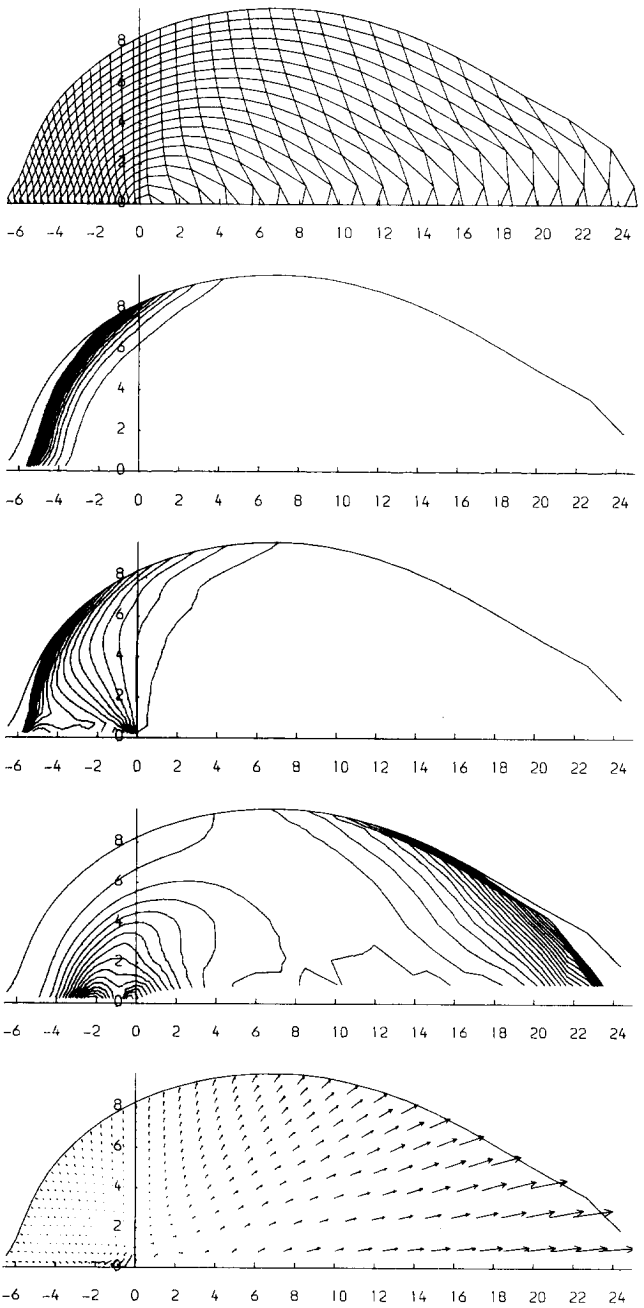

FIG. 3. As in Fig. 2 with LP code.

far as possible. Of course, it is only the Cartesian components of momentum which are conserved and so there will inevitably be a source term for the ϖ momentum component. This is the reason why we shall not consider the x and y velocity components, but u_ϖ and u_z.

Begin by defining a four component vector, φ, and three four component functions of φ as follows:

$$\varphi = \begin{bmatrix} \rho \\ \rho u_\varpi \\ \rho u_z \\ E \end{bmatrix}; \quad F(\varphi) = \begin{bmatrix} \rho u_\varpi \\ \rho u_\varpi^2 + p \\ \rho u_\varpi u_z \\ u_\varpi(E+p) \end{bmatrix}, \quad G(\varphi) = \begin{bmatrix} \rho u_z \\ \rho u_\varpi u_z \\ \rho u_z^2 + p \\ u_z(E+p) \end{bmatrix}, \quad S(\varphi) = \begin{bmatrix} 0 \\ p \\ 0 \\ 0 \end{bmatrix},$$

where

$$E = \frac{1}{2}\rho(u_\varpi^2 + u_z^2) + \frac{p}{\gamma - 1}.$$

All the symbols have their usual meaning. F and G are the ϖ and z flux vectors for Cartesian coordinates and S is a source vector. Note that the variables ρ, u_ϖ, u_z, p and E are acting merely as parameters to define F, G and S in terms of φ. Note also that F, G and S are homogeneous functions of φ, that is, $F(\alpha\varphi) = \alpha F(\varphi)$ for any number α. The axisymmetric equations of motion are

$$\frac{\partial \hat{\varphi}}{\partial t} + \frac{\partial}{\partial \varpi}(F(\hat{\varphi})) + \frac{\partial}{\partial z}(G(\hat{\varphi})) = \frac{S(\hat{\varphi})}{\varpi},$$

where

$$\hat{\varphi} = \varpi\varphi.$$

We now consider a general time-dependent transformation, $z = z(x, y, t)$ and $\varpi = \varpi(x, y, t)$, into the computational variables x and y. After some algebra the equations become

$$\frac{\partial \varphi^*}{\partial t} + \frac{\partial H_x}{\partial x} + \frac{\partial H_y}{\partial y} = \frac{S(\varphi^*)}{\varpi}, \tag{1}$$

where

$$\varphi^* = J\hat{\varphi} = \varpi J\varphi, \tag{2}$$

$$J = \frac{\partial(z, \varpi)}{\partial(x, y)} = \frac{\pi}{2}R^2,$$

$$H_x(\varphi^*, x, y, t) = h_{x1}F(\varphi^*) + h_{x2}G(\varphi^*) + h_{x3}\varphi^* \tag{3}$$

and similarly for H_y. The coefficients are given by

$$h_{x1} = -\frac{1}{J}\frac{\partial z}{\partial y} = -\frac{1}{R^2}\frac{\partial}{\partial \theta}(R\cos\theta),$$

$$h_{x2} = \frac{1}{J}\frac{\partial \varpi}{\partial y} = \frac{1}{R^2}\frac{\partial}{\partial \theta}(R\sin\theta),$$

$$h_{x3} = \frac{1}{J}\frac{\partial(z,\varpi)}{\partial(y,t)} = -\frac{dz_0}{dt}h_{x2} - \frac{x}{R}\frac{\partial R}{\partial t},$$

$$h_{y1} = \frac{1}{J}\frac{\partial z}{\partial x} = \frac{2}{\pi R^2}\left(R\cos\theta + \left(\frac{\pi}{2}-\theta\right)\frac{\partial}{\partial\theta}(R\cos\theta)\right),$$

$$h_{y2} = -\frac{1}{J}\frac{\partial \varpi}{\partial x} = -\frac{2}{\pi R^2}\left(R\sin\theta + \left(\frac{\pi}{2}-\theta\right)\frac{\partial}{\partial\theta}(R\sin\theta)\right),$$

$$h_{y3} = \frac{1}{J}\frac{\partial(z,\varpi)}{\partial(t,x)} = -\frac{dz_0}{dt}h_{y2} + \frac{2x}{\pi R}\left(\frac{\pi}{2}-\theta\right)\frac{\partial R}{\partial t}.$$

Note that the fluxes H_x and H_y are still homogeneous functions of φ^*.

To sum up, we have found that the natural variables are the φ^* defined by (2) and which vanish on the axis, $\varpi = 0$. Their fluxes are linear combinations of themselves and the Cartesian fluxes with coefficients consisting of derivatives of the transformation as given by (3). The next task is to find a robust way of solving system (1).

4. The Difference Scheme

Our first attempts to discretise (1) were a continuation of our previous experience with FCT-SHASTA. Zalesak [8] gives a clear acount of how to construct quite general Flux Corrected Transport (FCT) algorithms from high- and low-order difference schemes and gives a flux correction procedure applicable in multidimensions. We used a simple diffused–antidiffused Lax–Wendroff scheme, but found it to be very unstable, particularly near the axis. It seems that some care is needed in choosing the correct method for particular problems when using FCT techniques and since it was not clear how to proceed with this in our case it was decided to experiment with a different approach which has fewer free parameters, namely, flux splitting.

The flux splitting method is an attempt to take account of the way information is propagated at the characteristic velocities, that is, the eigenvalues of the Jacobian matrix $\partial H/\partial\varphi$. In one spatial dimension differential forms exist which are zero along characteristics (and integrable for homentropic flow leading to Riemann invariants). The situation is more complicated in multidimensions, as described by Butler [9], for example, and an alternative method is flux splitting, an idea which is also related to

the Godunov approach to the numerical solution of hyperbolic equations, as discussed by an Albada, van Leer and Roberts [10]. One writes $H = H^+ + H^-$, where H^+ is the flux due to information travelling in the positive direction in the relevant coordinate. However, it should be emphasized that there is no direct mathematical justification for flux splitting since there is not a part of the flux which is directly due to effects associated with each characteristic. Thus any method is somewhat arbitrary and should be judged on how it performs.

The method actually used is described by Steger and Warming [11] and depends on the homogeneity of H_x and H_y in φ. Because of this

$$H(\varphi) = \frac{\partial H}{\partial \varphi}\varphi.$$

Now $\partial H/\partial\varphi$ can be expressed as a sum

$$\frac{\partial H}{\partial \varphi} = \sum_n u_n C_n R_n = \sum_n M_n,$$

where C_n and R_n are a set of normalised eigencolumns and eigenrows of $\partial H/\partial\varphi$, that is,

$$\frac{\partial H}{\partial \varphi} C_n = u_n C_n, \qquad R_n \frac{\partial H}{\partial \varphi} = u_n R_n, \qquad R_m C_n = \delta_{mn}.$$

We can then simply put

$$H(\varphi) = H^+(\varphi) + H^-(\varphi),$$

where

$$H^+(\varphi) = \sum_{\{n \mid u_n > 0\}} M_n \varphi$$

and similarly for $H^-(\varphi)$. The actual calculation of the eigenvectors for the linear combination (3) is straightforward (after a little practice) and with some care the calculation of $H^+(\varphi)$ or $H^-(\varphi)$ for a given state φ can be reduced to a minimum for the various subsonic and supersonic cases. Alternatively, the formulae for the fluxes can be taken directly from the Steger and Warming paper [11].

With a method for flux splitting we can proceed analogously to the way described by van Albada *et al.* [10]. Given a set of φ (dropping the $*$) at time level k on the grid, $\varphi^k_{i,j}$, we use an averaging function to get values for $\partial\varphi/\partial x$, $\partial\varphi/\partial y$, $\partial H_x/\partial x$, $\partial H_y/\partial y$ in each cell. Typically

$$\left.\frac{\partial \varphi}{\partial x}\right|^k_{i,j} = \frac{1}{\delta x}\,\mathrm{ave}(\varphi^k_{i+1,j} - \varphi^k_{i,j}, \varphi^k_{i,j} - \varphi^k_{i-1,j}),$$

$$\left.\frac{\partial H_y}{\partial y}\right|^k_{i,j} = \frac{1}{\delta y}\,\mathrm{ave}(H(\varphi^k_{i,j+1}) - H(\varphi^k_{i,j}), H(\varphi^k_{i,j}) - H(\varphi^k_{i,j-1})).$$

The averaging function is

$$\text{ave}(a, b) = \frac{b^2 a + a^2 b}{a^2 + b^2}$$

as described by van Albada *et al.* with their bias set equal to zero to avoid bothering with a free parameter. The average is applied component by component. Experiments with simple one- and two-dimensional problems were made with the method and it was not found that the insertion of a bias, or vector-wise averaging, had any great effect. States are then defined at each of the four boundaries of the cell at the $k + \frac{1}{2}$ time level, and also at the cell centre. For compactness of notation these states are denoted by $\varphi^{k+1/2}_{i\pm,j}$, $\varphi^{k+1/2}_{i,j\pm}$, $\varphi^{k+1/2}_{i,j}$, where, for example, $\varphi^{k+1/2}_{i+,j}$ is the value of φ midway between i, i and $i+1$, i evaluated from the properties in the i, i cell. Thus it

Then write

$$H^{k+1/2}_{x\, i+1/2,j} = H^{+}_{x}(\varphi^{k+1/2}_{i+,j}) + H^{-}_{x}(\varphi^{k+1/2}_{i+1-,j})$$

and similarly for H_y so that eventually

$$\varphi^{k+1}_{i,j} = \varphi^{k}_{i,j} - \frac{\delta t}{\delta x}(H^{k+1/2}_{x\, i+1/2,j} - H^{k+1/2}_{x\, i-1/2,j})$$

$$- \frac{\delta t}{\delta y}(H^{k+1/2}_{y\, i,j+1/2} - H^{k+1/2}_{y\, i,j-1/2}) + \delta t \frac{S(\varphi^{k+1/2}_{i,j})}{\varpi^{k+1/2}_{i,j}}.$$

The whole scheme may then be coded on our triangular x, y grid. The greatest complication is in calculating the h coefficients in the sum (3) at the appropriate time levels, taking the grid distortion into account.

The time step is determined from the characteristic speeds of the H_x and H_y and a Courant number, K, assuming a generalised CFL condition:

$$\delta t = K \left\{ \min_{i,j} \left(\min \left\{ \frac{\delta x}{\max_n |u_n(H_x)|}, \frac{\delta y}{\max_n |u_n(H_y)|} \right\} \right) \right\},$$

where $u_n(H)$ stands for the nth eigenvalue of $\partial H/\partial \varphi$, as described above.

5. Boundary Conditions

In addition to the usual function of providing boundary values for the physical variables, the boundary conditions also determine how the grid evolves via

consistency conditions. In what follows we restrict ourselves to the case of a shock propagating into a medium with known properties but the way to generalise to other situations should be clear.

If the position of the shock is known at all times, then the Rankine–Hugoniot conditions can be solved to give the values immediately behind the shock. In our transformed variables, with the shock lying at $x = 1$, they are simply

$$[H_x] = 0.$$

This reflects the fact that all four characteristics enter the shock from in front. But there is also one characteristic which arrives from behind and it is the information obtained from this that determines the velocity of the shock. This velocity enters the definition of H_x (3) via h_{x3}.

It is not immediately clear how this consistency condition should be incorporated into the code. In one spatial dimension, one can obtain a relationship between the post-shock gradients and the shock acceleration, but it is simpler to try to use a time integrated version of this. This we do by equating the H_x^+ determined from the internal variables to that obtained from the shock conditions. It can be seen from (4) that H_x^+ is a projection of H_x onto the appropriate eigencolumn, C^+:

$$H_x^+(\varphi) = M^+(\varphi)\varphi = C^+(\varphi)\, R^+(\varphi)\, H_x(\varphi)$$

so that

$$R^+(\varphi)\, H_x^+(\varphi) = R^+(\varphi)\, H_x(\varphi) = R^+(\varphi)\, H_x(\varphi_0).$$

Here M^+, C^+ and R^+ have the same meaning as in the previous section, and apply to the characteristic entering the shock from behind; φ_0 is the state of the material in front of the shock. It may be noted that this shows that flux splitting is equivalent to the expansion of the flux as a sum of eigenvectors of $\partial H/\partial\varphi$. Thus the homogeneity property is not required if this definition is used. In any case the discretised form of the boundary condition is (referring to the definitions of the previous section)

$$R^+(\varphi_{N+,j}^{k+1/2})\, H_x^+(\varphi_{N+,j}^{k+1/2}) = R^+(\varphi_{N+,j}^{k+1/2})\, H_x(\varphi_{0,j}^{k+1/2}).$$

This is a linear scalar equation for dR/dt at the $k + 1/2$ time level. The specification is completed by

$$R_j^{k+1} = R_j^k + \delta t \left.\frac{dR}{dt}\right|_j^{k+1/2},$$

$$\left.\frac{dR}{dt}\right|_j^{k+1} = 2\left.\frac{dR}{dt}\right|_j^{k+1/2} - \left.\frac{dR}{dt}\right|_j^{k}.$$

Finally we need to impose conditions on the axis $y = \pm x$. These are trivial for the functions φ^* and the fluxes H_x and H_y since they are zero there. In fact the cells are arranged so that the axis cuts the cell sides at their midpoints (rather than their

corners) at 45° on the computational grid. Thus we have series of cells for which the boundary conditions give two of the fluxes as zero although the value of φ^* itself is not zero as the cell centre does not lie on the boundary. Again, the situation is illustrated at the top of Fig. 1. Thus a simple estimate of the gradient in these cells suffices to evaluate the remaining two fluxes. Note also that there is one cell, near the origin, which has three zero fluxes which can be treated similarly. This prescription has the advantage of being reasonably staightforward, but it is rather crude, and better results might be obtained with some kind of matching procedure.

We now have a complete description of our code and it remains to describe the results obtained with it.

6. The Results

For simplicity we consider a set of problems with only one free parameter: the scale height of a cold exponential atmosphere, z_H. Thus we consider the following set of initial and boundary conditions:

$$\varphi_0 = \begin{bmatrix} 1 \\ 0 \\ 0 \\ 0 \end{bmatrix} \exp\left(-\frac{z}{z_H}\right), \qquad \varphi(t=0) = \begin{bmatrix} 4 \\ 3\varpi \\ 3z \\ \frac{9}{8}(1+r^2) \end{bmatrix} \exp\left(-\frac{z}{z_H}\right),$$

$$R(\theta, 0) = 1, \qquad \frac{\partial R}{\partial t}(\theta, 0) = 1.$$

Note that the initial conditions are chosen so as to satisfy the shock conditions. This configuration is allowed to evolve from $t = 0$ to $t = 50$ with various values of z_H. We shall show here the results for two cases: $z_H = \infty$, to see how closely the scheme represents a spherical explosion, and $z_H = 2$, to model the effect of a density variation. In both cases we take $\gamma = \frac{5}{3}$.

In Fig. 1 and 2 show the computational grid, contour plots of density, temperature and pressure and velocity plots for $z_H = \infty$ and $z_H = 2$, respectively. The runs were done with Courant number $K = 0.5$ and 148 time steps were needed for Fig. 1 and 159 for Fig. 2. These runs took about 100 s on the Leeds University Amdahl V7A computer. About 60% of this is spent in calculating the mapping so that by using a cheaper method for this, and with more efficient programming, we feel that these times could easily be halved.

Figure 1 shows that the spherical property has been well preserved. The total variation in radius is about 3% and all but five points at each end lie within a 1% range. This shows the general stability of the code and the mapping. The higher inaccuracy at the points near the axis is one aspect of a general phenomenon that the results are rather erratic there; see particularly the pressure plot. This is due to the $\varphi = \varphi^*/\varpi J$ relationship which means we have to divide by ϖ to get the plotted

variables from the computational variables. Thus inaccuracies near the axis are to be expected, but should not affect the overall accuracy of the code. It turns out also that the time step is determined by cells near the axis and as a consequence it oscillates slightly. However, runs in which the time step was prescribed smoothly as a function of time gave essentially identical results, so this effect is also not important.

Turning now to Fig. 2, we see that the results are qualitatively as expected with the explosion having broken out to the right, in the direction of lower density. The highest densities and pressures are observed behind the shock moving into the dense material (the maximum preshock density is about 21), whereas the highest temperature and velocities are behind the right-moving shock (the minimum preshock density is about 2×10^{-5} at this time). Note that the stagnation point is around $z = -4$ but that the material initially forming the explosion has been pushed to the right and become prolate to the axis. Inspection of an entropy plot (not entirely reliable since shocks have propagated) suggests that this material is now centred around $z = 8$. We now try to get a more quantitative check on the results by following the procedure outlined in Section 1.

The first stage is to adjust our code to the LP method and we reduce the equations to the appropriate form in Appendix A. The differences are changes in the definition of the h coefficients of (3) and the appearance of a source for the z-momentum. These changes are easily incorporated and the results, for $z_H = 2$, are shown in Fig. 3. The results are similar, but reveal differences in detail. For example the multivalued pressure at the origin, implicit in the LP method, is clearly illustrated. It can be seen that the axial inaccuracy has caused bulges in the shock shape on the axis which are more pronounced than for the correct equations. This is also true of a spherical LP calculation and it appears that the problem is greater for this method, possibly due to the z-momentum source.

A first check on the code is that the velocities should be radial and this can be seen to be the case in Fig. 3. A detailed check consists in verifying that the structure along each radius is the same as that in the equivalent spherical model. We have made "exact" spherical calculations with a one-dimensional version of the code with superior resolution. In Fig. 4 we compare the temperature structure along the ϖ axis. In these spherical calculations a compression wave is propagated inwards from the initial position of the outer shock and eventually steepens into a further shock. This reflects from the centre and moves steadily outwards. The continuous line in Fig. 4 is the accurate temperature structure and shows a plateau. The temperature rises inside this plateau because the shock is very strong on initial reflection and decays as it moves out. It falls outside the plateau because the outer shock is slowing down. The plateau has been diffused by the low resolution calculations (in one dimension and the LP method) as one would expect but otherwise the agreement is good with the LP calculation, in fact doing slightly better than the one-dimensional spherical calculation with the same resolution. Figure 4 also shows the temperature structure along the ϖ axis for the correct two-dimensional equations and it can be seen that this is completely different from what is obtained by the LP method, indicating a different shock history.

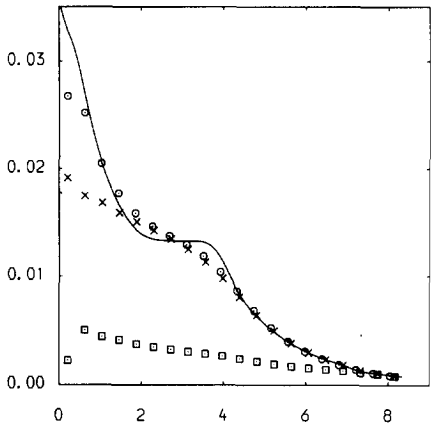

FIG. 4. Temperature structure along the ϖ axis from various calculations Continuous line: one dimensional with 100 cells. Crosses: one dimensional with 20 cells. Circles: two dimensional LP calculation with 20 radial cells. Squares: two dimensional correct calculation with 20 radial cells.

Finally we run the problem for a problem with a known analytic LP solution. This is described in Appendix B. The principal features of the density distribution are that it becomes infinite at $z = -(0.03)^{-2/3} \simeq -10.36$ and that it decays to zero in the other directions. The explosion hits the singularity in a finite time, $t \simeq 45.778$, and so we look at the results at $t = 45$. In Figures 5 and 6 we show respectively the solution obtained with the LP code and the LP exact solution. In Figure 7 we make a more detailed comparison by plotting the radius against position angle for each model. It can be seen that the agreement is good, except on the axis which we know to be not well treated. The contour diagrams, too, show that the details are essentially correct

7. CONCLUSION

We have described a code which solves axisymmetric free boundary problems for hyperbolic systems with great economy and considerable simplicity. We have tried to show that results of reasonable accuracy are obtained, though this is hard in an area which is intractable analytically. At any rate the economy shows that good resolution may be obtained, if desired, and the simplicity shows that extensions to more complicated problems can be made straightforwardly. For example we might want to study the interaction of an explosion with a rigid wall, or we could match onto some other solution at the boundary along the lines described in Section 1. Although the principal motivation for the work is the study of explosive phenomena in a non-uniform astrophysical medium, there must be many other areas in which the approach would be successful.

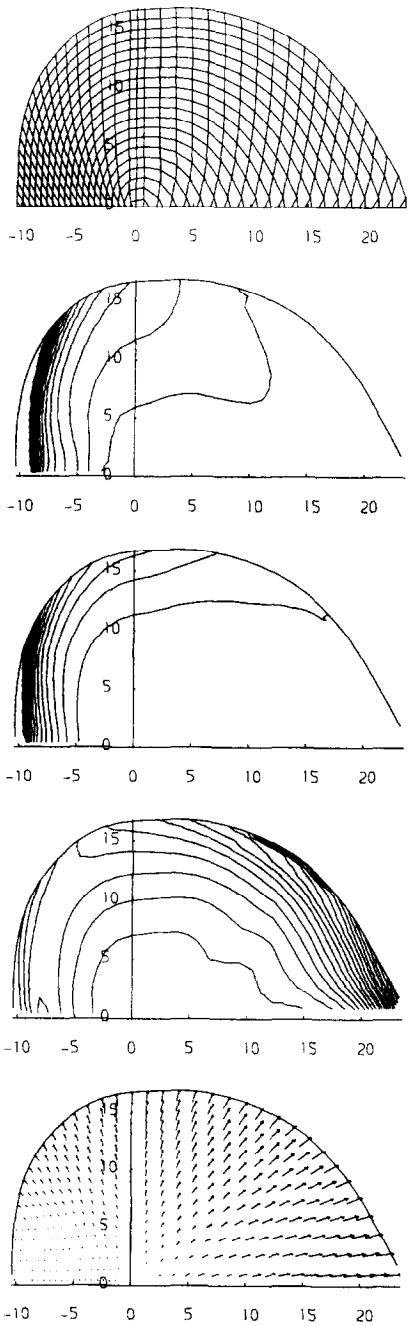

FIG. 5. As Figs. 1–3 for analytic LP problem. Contour units are now 0.005 for density, 0.00005 for pressure and 0.002 for temperature.

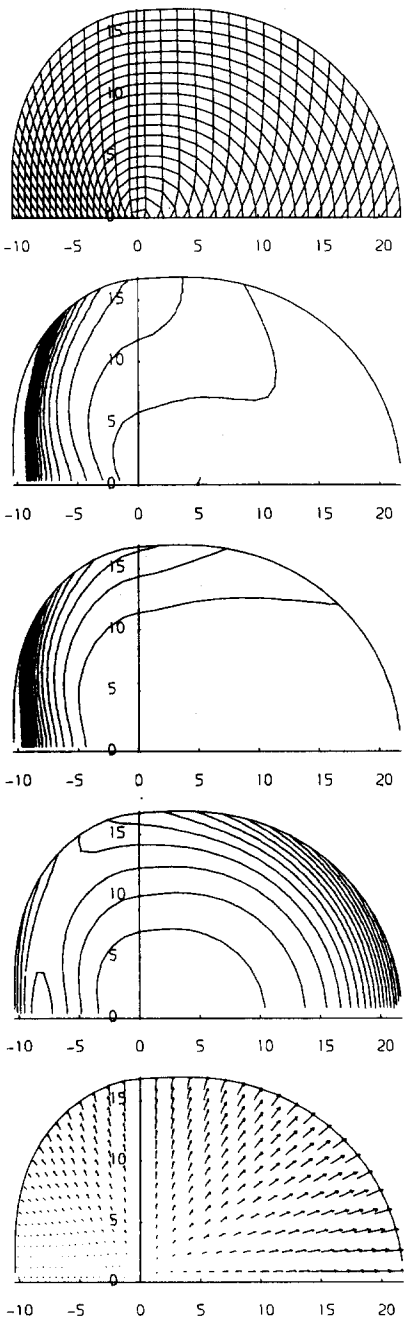

FIG. 6. Analytic solution to LP problem drawn as in Fig. 4.

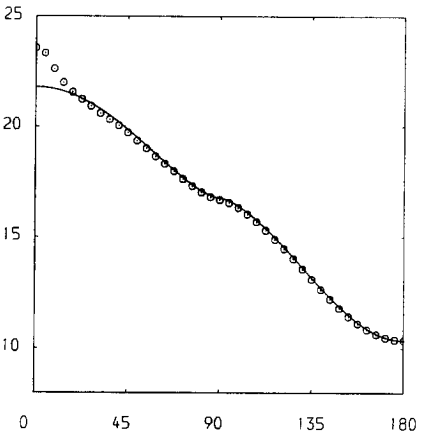

FIG. 7. Radius, $R(\theta)$, drawn against angle for the analytic LP problem. The continuous line is the analytic solution of Fig. 5 and the circles are obtained from the LP code results of Fig. 4.

An important point which has emerged from the work is the reliability and accuracy of the flux splitting method. The development of the code has involved several programs utilising this method to solve simple one-dimensional problems, one-dimensional analogues of the present scheme and two-dimensional wind tunnel problems. In all cases satisfactory results were obtained with no need for fine tuning of any kind. It is clear that working with the transformed equations makes great demands on the algorithms and that flux splitting works because it uses both the conservative properties and the characteristic relations in such a way as to make the discretised equations as fluid-like as possible. A useful consequence is that boundary conditions can be applied in an essentially routine way, with due account given to characteristics entering and leaving the grid. Presumably, even better results will be possible when the method has been further improved and refined. For example there may be superior ways in which the flux can be split and certainly the treatment of the source terms, rather crude here, could be enhanced. And for the present problem some method for improving the results near the axis would be desirable.

We conclude with some remarks about the usefulness of the LP method. Figures 2 and 3 for the exponential atmosphere show that although the LP method gives qualitative agreement with the results obtained with the correct equations, the detailed distributions of temperature and pressure are quantitatively wrong. However it turns out that for the analytic LP problem the results using the correct equations are very close to the LP solution. This may be partly because the pressure becomes zero at the centre for this problem and so is not multivalued in the LP approach which thus avoids one of its most obvious failings. We conclude that the LP method can give a rough picture of the evolution of an explosion which becomes less accurate as the explosion extends over more scale heights. However it is not capable of giving a reliable picture of the structure of the explosion, though its shape is one of the properties better modelled. None of this is very surprising.

APPENDIX A: THE LP EQUATIONS

The LP method is described by the usual spherical equations, with the proviso that the functions depend on θ. That is:

$$\begin{aligned}
&\frac{\partial}{\partial t}(r^2\rho) + \frac{\partial}{\partial r}(r^2\rho u_r) = 0,\\
&\frac{\partial}{\partial t}(r^2\rho u_r) + \frac{\partial}{\partial t}(r^2(\rho u_r^2 + p)) = 2rp,\\
&\frac{\partial}{\partial t}(r^2 E) + \frac{\partial}{\partial r}(r^2 u_r(E + p)) = 0.
\end{aligned} \tag{A1}$$

It is useful to define the vector

$$P(\varphi, \theta) = \sin(\theta)\, F(\varphi) + \cos(\theta)\, G(\varphi) = \begin{bmatrix} \rho u_r \\ \sin(\theta)(p + \rho u_r^2) \\ \cos(\theta)(p + \rho u_r^2) \\ u_r(E + p) \end{bmatrix}$$

with the same parameterisation as before in terms of u_ϖ and u_z and where

$$\begin{aligned}
u_\varpi &= u_r \sin\theta,\\
u_z &= u_r \cos\theta.
\end{aligned}$$

The appropriate equations for $\hat{\varphi} = \varpi\varphi$ are then

$$\frac{\partial\hat{\varphi}}{\partial t} + \frac{\partial}{\partial\varpi}(\sin(\theta)\, P(\hat{\varphi}, \theta)) + \frac{\partial}{\partial z}(\cos(\theta)\, P(\hat{\varphi}, \theta)) = \frac{2\hat{p}\sin(\theta)}{\varpi} \begin{bmatrix} 0 \\ \sin\theta \\ \cos\theta \\ 0 \end{bmatrix}.$$

Applying the mapping to obtain the equation for φ^* we obtain new h coefficients in terms of the old ones:

$$\begin{aligned}
h_{1\mathrm{LP}} &= \sin(\theta)(h_1 \sin\theta + h_2 \cos\theta),\\
h_{2\mathrm{LP}} &= \cos(\theta)(h_1 \sin\theta + h_2 \cos\theta).
\end{aligned}$$

In the sources, the column vector $(0\ 1\ 0\ 0)^T$ is replaced by $(0\ 1{-}\cos 2\theta\ \sin 2\theta\ 0)^T$.

APPENDIX B: THE ANLYTIC LP PROBLEM

We need to find an analytic solution to the spherical equations (A1). We do this by demanding

$$u_r(r, \theta, t) = U(\theta, t)\, r.$$

The continuity and energy equations are satisfied by solutions of the form

$$\rho = f^{-3} D(\xi), \qquad p = f^{-5} P(\xi), \qquad \xi = \frac{r}{f}, \quad f = \exp\left(\int_0^t U\, dt\right).$$

We are assuming $\gamma = \frac{5}{3}$ and ξ is a Lagrangian variable. The momentum equation then requires (in separable form)

$$f^3 \frac{\partial^2 f}{\partial t^2} + \frac{1}{\xi D}\frac{dP}{d\xi} = 0.$$

The separated equations can then be solved and when the solution is fitted to a shock moving into cold material we find the density must be of the form

$$\rho_0(r) = \frac{1}{ar^2(1 + br^{3/2})^{3/2}},$$

where a and b are constants. As before we take the initial shock radius and velocity both to be one, for which

$$f^2 = 1 + \frac{3}{2}t + \frac{9bt^2}{16(1+b)},$$

and the shock radius is $R_s = f^{4/3}$. The functions D and P are given by

$$D(\xi) = \frac{4\xi}{a(1 + b\xi^6)^{3/2}}$$

$$P(\xi) = \frac{3\xi^3}{4a(1+b)(1+b\xi^6)^{1/2}} \qquad \text{for} \quad \xi \geqslant 1.$$

We also take this to be the solution for $\xi < 1$, that is, for gas that is not shocked. Note that if $-1 < b < 0$ the density becomes infinite and the singularity is reached at time $t = 4(1+b)/(-3b)$.

We now arrange that a and b be functions of θ to give a complete LP problem and choose them as follows:

$$b = 0.03\ \text{sign}(\cos\theta)\,|\cos\theta|^{3/2},$$

$$a = (1+b)^{-1}.$$

These have the effect that the density becomes infinite on the plane $z = -(0.03)^{-2/3}$ and that each solid angle contains the same amount of energy, the LP assumption for a point explosion, which is violated for our initial conditions for the exponential atmosphere.

REFERENCES

1. S. A. E. G. FALLE, *Monthly Not. Roy. Astron. Soc.* **195** (1981), 1011.
2. A. R. GARLICK, *Astrophys. Space Sci.* **84** (1982), 205.
3. S. A. E. G. FALLE AND A. R. GARLICK, *Monthly Not. Roy. Astron. Soc.* **201** (1982), 635.
4. D. L. BOOK, J. P. BORIS, AND K. HAIN, *J. Comput. Phys.* **18** (1975), 248.
5. R. A. CHEVALIER AND J. GARDNER, *Astrophys. J.* **192** (1974), 457.
6. D. D. LAUMBACH AND R. F. PROBSTEIN, *J. Fluid Mech.* **35** (1969), 53.
7. D. I. MEIRON, S. A. ORSZAG, AND M. ISRAELI, *J. Comput. Phys.* **40** (1981), 345.
8. S. T. ZALESAK, *J. Comput. Phys.* **31** (1979), 335.
9. D. S. BUTLER, *Proc. Roy. Soc. A* **255** (1960), 232.
10. G. D. VAN ALBADA, B. VAN LEER, AND W. W. ROBERTS, *Astron. Astrophys.* **108** (1982), 76.
11. J. L. STEGER AND R. F. WARMING, *J. Comput. Phys.* **40** (1981), 263.